Proceedings of International Conference on Heat Exchanger Fouling and Cleaning - 2011 (Peer-reviewed)
June 05 - 10, 2011, Crete Island, Greece
Editors: M.R. Malayeri, H. Müller-Steinhagen and A.P. Watkinson

Published online
www.heatexchanger-fouling.com

CFD MODELLING OF ASH DEPOSITS IN COAL-FIRED POWER PLANTS

A. Magda, S.I. Magda, M. Strelow, H. Müller and R. Leithner

Institut für Wärme- und Brennstofftechnik,
Technische Universität Braunschweig

Franz-Liszt-Straße 35, 38106, Braunschweig, Germany

E-mail: a.magda@tu-bs.de

ABSTRACT

In order to understand the mineral transformation and deposit formation, a small size coal combustion test facility fired with pulverized Hambach coal was investigated experimentally and by computational fluid dynamics (CFD). Emphasis was placed on chemical characterization of coal, mineral matter (MM) and deposits. The transformation of individual minerals was modeled based on kinetic data.

1 INTRODUCTION

The prediction of fouling and slagging by means of empirical indices is still a common practice among power plants operators. At their best they deliver satisfactory results, but suffer from the lack of information on ash-particle dynamics and facility operational and geometrical features. A recent study aiming at improving the slagging index by considering the volumetric load failed to establish a correlation between the aforementioned parameters (Bonn, 2010).

Commonly, ash depositions tools are appended as post-processors to CFD-simulation programs. They address comprehensively the ash-coal particle dynamics, MM redistribution, ash formation mechanisms, ash transport and deposit growth (Hecken et al., 2001), (Richards et al., 1993), (Yan et al., 2002), (Lee and Lockwood, 1998), (Erickson et al., 1995), (Wilemski and Srinivasachar, 1993), but ignore the MM transformation along the particle trajectory and deposit chemistry. The reason for this simplification is that kinetic data for MM transformations in coal-fired boilers are rarely available in literature.

2 MATHEMATICAL MODELING

The FLOREAN package has been used to simulate the pulverized coal combustion (Müller, 1992), (Leithner et al., 2003a,b). A Lagrangian based post processor is used for the particle tracking (Fischer, 1998), (Bozic, 2003), (Magda et al., 2009). Each particle is considered as a miniature chemical reactor. For each time-step along with specific coal combustion processes, e.g., drying, devolatilization, volatiles and char combustion, an additional MM transformation module is accessed.

The basis of Lagrangian approach to two-phase flows is the simulation of the particle trajectory by tracking representative parcels of particles. The particles are initialized and released from a finite number of starting locations and tracked throughout the computational domain. Accounting the forces acting on the particle it is possible to predict the particle position and behavior at each instant. By considering energy sink and source terms for conduction, convection, radiation and chemical activity the particle thermal state is described. The one-way coupling method is applied (Bozic, 2003).

2.1 Particle motion

The particle motion is expressed as a function of drag and gravitational forces, neglecting forces like the added mass force or thermophoresis. Constant particle mass is assumed during each time step (Fischer, 1998), (Wörner, 2003):

$$m_p \frac{d\bar{u}_p}{d\tau} = \frac{1}{2}\rho_g A_{pcs} C_D \left|\bar{u}_g - \bar{u}_p\right| \cdot \left(\bar{u}_g - \bar{u}_p\right) + V_p\left(\rho_p - \rho_g\right)\bar{g} \quad (1)$$

The particle velocity is calculated as (Lockwood et al., 1995):

$$\bar{u}_p(\tau+\Delta\tau) = \bar{u}_g(\tau) + \tau_p \cdot \bar{g} + \left[\bar{u}_p(\tau) - \bar{u}_g(\tau) - \tau_p \cdot \bar{g}\right] \cdot exp\left(-\frac{\Delta\tau}{\tau_p}\right) \quad (4)$$

The particle is assumed to be spherical so that the experimental results for the drag coefficient of a solid sphere can be applied (Schiller and Nauman, 1935), (Schubert, 1977).

The particle trajectory is obtained by integrating the equation:

$$\frac{dx_{p,i}}{d\tau} = u_{p,i} \quad (5)$$

The new particle position is calculated as:

$$x_p(\tau+\Delta\tau) = x_p(\tau) + \frac{1}{2}\left[\bar{u}_p(\tau) + \bar{u}_p(\tau+\Delta\tau)\right]\Delta\tau \quad (6)$$

2.2 Coal particle combustion

Changes in coal particle composition are due to moisture vaporization, pyrolysis, char combustion and MM transformation.

Moisture release starts once the coal particle enters the furnace. The water content is readily vaporized by means of heat by radiation, convection and conduction.

A simple model for moisture release was proposed by McIntosh (1976):

$$\frac{dm_{H_2O}}{d\tau} = \dot{m}_{H_2O} = -\frac{\dot{Q}_{conv} + \dot{Q}_{rad}}{r_{H_2O}} \tag{7}$$

With further temperature increase devolatilization takes place, releasing volatiles and leaving over char. The mass balance for a single coal grain is:

$$\frac{dm_{coal,daf}}{d\tau} = \frac{dm_{coal}^{pyr}}{d\tau} = -\frac{dm_{vol}^{pyr}}{d\tau} - \frac{dm_{char}^{pyr}}{d\tau} \tag{8}$$

$$\frac{dm_{vol}^{pyr}}{d\tau} = -\nu \frac{dm_{coal,daf}}{d\tau} \tag{9}$$

$$\frac{dm_{char}^{pyr}}{d\tau} = -(1-\nu)\frac{dm_{coal,daf}}{d\tau} \tag{10}$$

The stoichiometric coefficient ν is calculated based on the proximate volatile matter content.

The rate of coal devolatilization is described by:

$$\frac{dm_{coal,daf}}{d\tau} = -K_{pyr} m_{coal,daf} \tag{11}$$

The devolatilization rate constant is based on experimental findings and is expressed in form of Arrhenius equation:

$$K_{pyr} = k_{0,pyr} \cdot exp\left(-\frac{E_{pyr}}{RT}\right) \tag{12}$$

Volatiles mix with the available oxygen and burn in the gaseous environment, serving as primary fuel for combustion. The char mass balance is composed of a source term accounting for the char produced during the pyrolysis and a sink term for the char combustion:

$$\frac{dm_{char}}{d\tau} = \frac{dm_{char}^{pyr}}{d\tau} - \frac{dm_{char}^{com}}{d\tau} \tag{13}$$

Char combustion is assumed to take place only at the particle-gas surface (external or porous structure) and considers diffusion and chemical reaction effects (Field and others, 1967).

$$C + \frac{1}{f_m} O_2 \rightarrow \left(2 - \frac{2}{f_m}\right) CO + \left(\frac{2}{f_m} - 1\right) CO_2 \tag{14}$$

The mechanism factor f_m in the above equation states that the burning char will produce only CO and CO_2 and accounts for the particle size influence. For large particles when only CO_2 is produced $f_m = 1$, while in case of fine particles when only CO is produced $f_m = 2$.

The char burnt within the particle is (Field and others, 1967):

$$\frac{dm_{char}^{comb}}{d\tau} = -m_{char} \cdot k_{char} \cdot a_p \cdot p_{O_2,\infty} \tag{17}$$

2.3 Particle heat balance

The energy balance for the coal particle is expressed as (Bozic, 2003):

$$\dot{Q}_p = \frac{dQ_p}{d\tau} = \dot{Q}_{chem} + \dot{Q}_{rad} + \dot{Q}_{cond} + \dot{Q}_{conv} + \dot{Q}_{mass} + \dot{Q}_{vap} + \dot{Q}_{mi} \tag{22}$$

$$\dot{Q}_{mi} = \frac{dQ_{mi}}{d\tau} = \dot{Q}_{mi,chem} + \dot{Q}_{mi,melt} + \dot{Q}_{mi,sol} + \dot{Q}_{mi,vap} + \dot{Q}_{mi,polym} \tag{23}$$

Using the Runge-Kutta-Fehlberg method the new temperature of the particle is calculated:

$$\frac{dt_p}{d\tau} = \frac{\dot{Q}_p}{m_p \cdot c_{p,p}} \tag{24}$$

2.4 Mineral matter transformation

The lack of adequate kinetic data most often limits the MM chemistry to equilibrium considerations, although criteria for equilibrium are not always fulfilled (Kingery et al., 1976).

In equilibrium analyses each particle is assumed to be a well-mixed chemical reactor and the fluid dynamics limitations (residence time, kinetic or diffusion, agglomeration and sintering are unable to retard the reaction rate (Zevenhoven and Backman, 2000)) are not taken into account. The system reflects a hypothetical state in which either the reactions themselves are very fast or the available time for their occurrence is large enough. The main advantage of the equilibrium approach consists in the possibility to calculate equilibrium and thermodynamic properties for a wide variety of multicomponent, multiphase systems and reactions.

The kinetic approach is mostly thought of as the appropriate approach. It has the disadvantage of being limited to very scarce kinetic data. The residence time, kinetic and diffusion effects, agglomeration and sintering, all very important for energy conversion systems can be accounted for through the reaction rate.

Ash deposition models in literature address either the coal-ash particle dynamics (Lee and Lockwood, 1998) or the MM chemistry (Wei et al., 2002), but a sound model needs to be constructed based on both mechanisms (Bozic, 2003).

2.4.1 Mineral database

The complexity and variability of the coal mineralogy point towards the use of a chemical mechanism that accounts for as many as possible chemical compounds and interactions. Reliable and accurate thermochemical data are therefore needed.

For this purpose a coal and biomass database BICOD as text (csv) and as HTML was developed. The database contains 110 biomass and coal chemical analyses and 200 individual mineral species descriptions.

Each mineral description is subdivided into several subset databases. One subset refers to the polynomial format to calculate the mineral thermodynamic properties, e.g., H, S, c_p, (McBride et al., 1993). The reaction subset encompasses 140 reactions compiled from literature. The entries are indexed with the following subheadings: identification number, reactants and products, fit function model, fit function order, polynomial model, polynomial coefficients, temperature validity range, partial pressure of the reacting gas and literature source.

The database is available to public on request and can be easily extended to fit one's needs.

2.4.2 Mineral matter transformation kinetic solver

Kinetics is the study of the rates of chemical processes in an effort to understand what is that influences these rates and to develop theories which can be used to predict them.

Once they are built (as function of temperature, pressure, concentrations, particle diameter, etc.) these models are employed to perform calculations for any set of conditions.

A single n[th] order irreversible reaction can be represented by the general form:

$$v_{1,R}R_{C,1}+v_{2,E}R_{C,2}+\ldots \rightarrow v_{1,P}P_{R,1}+v_{1,P}P_{R,2}+\ldots \quad (25)$$

Assuming a physico-geometry based kinetic model function f(X) and the constant rate K, the following generic kinetic equation can be written (Epple et al., 2009):

$$\frac{dX}{dt}=K\cdot f(X) \quad (26)$$

Table 1 lists the kinetic model functions f(X) employed for the kinetic study of the solid-state reactions (Tanaka, 1995), (Vyazovkin and Wight, 1997).

Table 1 Kinetic model function f(X)

R1 - 1D PBC	1.0
R2 - 1D PBC	$2(1-X)^{1/2}$
R3 - 1D PBC	$3(1-X)^{2/3}$
D1 - 1D Difussion	$1/(2X)$
D2 - 2D Difussion	$-1/ln(1-X)$
D3 - 3D Diffusion (Jander)	$\frac{3(1-X)^{2/3}}{2\left(1-(1-X)^{1/3}\right)}$
D4 - 3D Diffusion (Ginstring-Brounshtein)	$\frac{3}{2}\cdot\frac{1}{(1-X)^{-1/3}-1}$
D5 - 3D Diffusion (Carter)	$\frac{\left[1+(Z-1)X\right]^{\frac{1}{3}}(1-X)^{1/3}}{\left[1+(Z-1)X\right]^{1/3}-(1-X)}, Z=V_p/V_{0,P}$
An - Nucleation	$n(1-X)\left[-ln(1-X)\right]^{(n-1)/n}$
Fn - Formal kinetic	$(1-X)^n$
B1 - Autocatalyst	$X(1-X)$
M - Melting fraction mass/volume	$X_{melt}=\frac{1}{m_{p,0}}\int_0^{\tau}\left(\frac{\dot{Q}_{con}+\dot{Q}_{rad}+\dot{Q}_{mi,chem}}{\Delta H_{melt}}\right)d\tau$
SCM	$X=1-(r/r_c)^3$ $\frac{dr}{d\tau}=\frac{-v_{1,R}}{v_{2,R}}\frac{M_{2,R(g)}}{\rho_1}k_{eff}C_{2(g)}$ $k_{eff}=\frac{1}{\frac{1}{k_{chem}}+\left(\frac{r}{r_c}\right)^2+\frac{r}{D^{eff}_{p,por}}\left(1-\frac{r}{r_c}\right)}$

Phase boundary controlled models **R1-R3** are used to describe reactions with non-porous core when diffusion processes are neglected and for evaporation, sublimation and dissolution. Diffusion models **D1** and **D2** are used to describe coalescence of MM inclusions in single ash particles. The **D3-D5** models are used to describe solid state diffusion of mineral powder mixtures in particles. Physical processes of crystallization, recrystallization and decomposition have been successfully fitted with the **An** model. Formal kinetic n[th] order model **Fn** describes heterogeneous reactions. When gas diffusion, Knudsen diffusion or some other diffusion processes and chemical reaction need to be taken into account the shrinking core model **SCM** is applied.

For all model functions it is assumed that the mineral unreacted core is nonporous, while the spherical shell enveloping the core can be porous (Bozic et al., 2000).

Table 2 Chemical reaction polynomials

P1	$K=\left[C_1\cdot\left(\frac{\beta_t}{\beta_{t,0}}\right)^{P_1}\cdot C_2\cdot\left(\frac{p_{O_2}}{p_0}\right)^{P_2}\cdot C_3\cdot\left(\frac{T}{T_o}\right)^{P_3}\cdot C_4 e^{\left(\frac{-C_5}{T}\right)^{P_4}}+C_0\right]$
P2	$K=C_1\cdot\left(\frac{\beta_t}{\beta_{t,0}}\right)^{P_1}+C_2\cdot\left(\frac{\beta_t}{\beta_{t,0}}\right)^{P_2}+C_3\cdot\left(\frac{\beta_t}{\beta_{t,0}}\right)^{P_3}$ $+C_4\cdot log\left(\frac{p_{O_2}}{p_0}\right)^{P_4}+C_5\cdot log\left(\frac{p_{O_2}}{p_0}\right)^{P_5}$ $+C_6\cdot\left(\frac{T}{T_0}\right)^{P_6}+C_7\cdot\left(\frac{T}{T_0}\right)^{P_7}+C_8\cdot\left(\frac{T}{T_0}\right)^{P_8}+C_9\cdot\left(\frac{T}{T_0}\right)^{P_9}+C_{10}\cdot\left(\frac{T}{T_0}\right)^{P_{10}}+C_0$
P3	$K=C_1 e^{(C_2\cdot T)^{P_2}}+C_0$
P4	$K=C_1\cdot T^{P_1}+C_2 e^{\left(\frac{-C_3}{T}\right)}+C_0$
P5	$K=C_1\cdot T^{P_1}\cdot e^{\left(\frac{-C_2}{T}\right)}+C_0$
P6	$K=C_1\cdot\left(\frac{\beta_t}{\beta_{t,0}}\right)^{P_1}\cdot\left[C_2\cdot\left(\frac{T}{T_0}\right)^{P_2}+C_3\cdot\left(\frac{T}{T_0}\right)^{P_3}+C_4\cdot\left(\frac{T}{T_0}\right)^{P_4}+C_5\cdot\left(\frac{T}{T_0}\right)^{P_5}\right]$
P7	$K=C_1\cdot\left(\frac{\beta_t}{\beta_{t,0}}\right)^{P_1}\cdot\left[C_2\cdot\left(\frac{p_{O_2}}{p_0}\right)^{P_2}+C_3\cdot\left(\frac{p_{O_2}}{p_0}\right)^{P_3}+C_4\cdot\left(\frac{p_{O_2}}{p_0}\right)^{P_4}+C_5\cdot\left(\frac{p_{O_2}}{p_0}\right)^{P_5}\right]$

The reaction constant depends on the Arrhenius parameters, temperature, activation energy, reactants to products ratio, partial pressure and particle diameter. The constant rate is characterized by the polynomial functions (P1-P7) presented in Table 2.

2.4.3 Mineral matter transformation and coal combustion coupling

The MM transformation procedure is appended to a Lagrangian module and is accessed at each time step. Based on the mineral species within the particle and the local environment the mineral reactions to occur are identified. Once the aforementioned procedure has been performed for all the minerals within the particle ones proceeds to the calculation of particle mass, density and specific heat.

A particle fusion temperature (PFT) criterion is used to model deposit growth. If the particle impaction temperature is higher than the PFT, the particle sticks to the wall and its trajectory is ended. Contrarily, the particles rebound and are further tracked.

3 PRACTICAL APPLICATION

3.1 Test facility description

The experiments were carried out in a pulverized solid fuel furnace with a maximal thermal output of 1 MW (Fig. 1). The thermal output, air and fuel mass flow rates are established function of fuel type and quality. The furnace consists of a horizontal combustion chamber and a swirl burner. The operation conditions are given in Table 3.

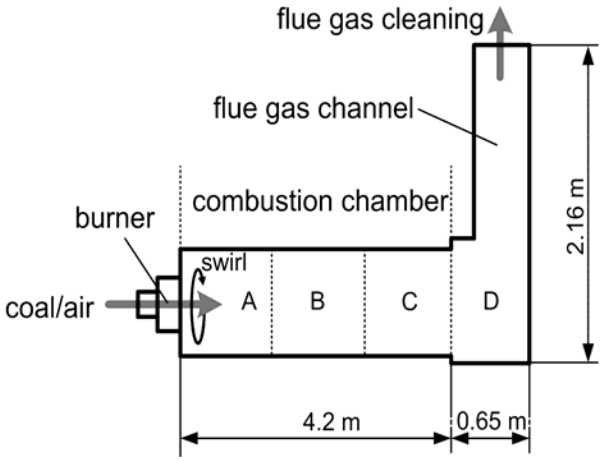

Fig. 1 Test facility

Table 3 Furnace inlet coal/air

	Temperature °C	Mass flow kg/s
Combustion air		
Conveying air	20	0.0200
Swirl air	190	0.0342
Secondary air	181	0.0236
Ternary air	204	0.1330
Coal	20	0.0231

Table 4 Hambach coal analyses

Particle size distribution					
Particle size µm	14	41	84	155	270
Fraction mass-%	20	20	20	20	20
Proximate analysis					
Moisture*	mass-%	11.50			
Volatile matter (daf)	mass-%	52.49			
Ash*	mass-%	3.91			
Heating value (daf)	MJ/kg	21.78			
Ultimate analysis mass-% (daf)					
C	H	N	S	O	
69.48	5.01	0.80	0.46	24.25	
Fraction of raw minerals per particle class mass-%					
Particle diameter µm	< 80	80-112	112-160	> 160	
Pyrite	0.15	0.22	0.00	0.28	
Quartz	0.96	0.10	0.10	0.02	
Hematite	0.28	1.57	0.07	1.17	
Periclase	8.55	4.31	10.35	15.17	
Siderite	0.69	17.32	1.76	26.62	
Gypsum	80.45	52.41	23.98	42.45	
Kaolinite	0.79	1.15	2.02	8.95	
Unidentified	8.13	22.92	61.72	5.34	
Sum	100	100	100	100	

* - after fuel drying in the mill

The furnace was fired with dried lignite from Hambach opencast coal mine. The ultimate, proximate, oxide analyses and raw MM distribution in particles are summarized in Table 4.

The furnace was operated for 27 h under nearly stationary conditions. At the end of the experiments, after cooling, the furnace was inspected for ash deposit formation. The entire amount of ash was collected and weighted. The rate of deposition was determined as the mass of the collected ash divided by the experiment time.

Regarding the ash quantification on each of the furnace walls only a visual evaluation was possible. Because of the low temperatures (< 1000 °C) only loose, powdery deposits are formed which due to perturbations either during combustion or ash collection procedure fall easily to the bottom wall.

Almost the entire amount of ash was gravitationally deposited on the bottom wall. Two ash hills, one in section A and one in section B of the bottom wall were identified. The formation of the ash hills is explained by the presence of heavy, coarse particles which tend to fall to the bottom wall as soon as they enter the combustion chamber and the effects of the swirl burner which projects coal particles to the wall.

3.2 Major mineral transformations of Hambach coal

Based on the coal chemical analysis (Table 4) the following chemical reactions are identified as having a major role in MM transformation of Hambach coal (Bozic, 2003), (Tomeczek et al., 2004), (Neuroth, 2007).

The reactions were computed under isothermal conditions, based on the mathematical models presented in Table 1 and Table 2.

Table 5 Relevant MM reactions in Hambach coal

1	$xFeS_2 + (2x-1)O_2 \rightarrow Fe_xS + (2x-1)SO_2$	F1, P1	-
2	$Fe_xS \rightarrow xFe + 0.5S_2$	F1, P1	Fig. 5
3	$Fe_3O_4 \rightarrow 3FeO + 0.5O_2$	F1, P1	-
4	$3Fe_2O_3 \rightarrow 2Fe_3O_4 + 0.5O_2$	-	-
5	$3Fe_2O_3 + CO \rightarrow 2Fe_3O_4 + CO_2$	-	-
6	$Fe_3O_4 + CO \rightarrow 3FeO + CO_2$	SCM	-
7	$3Fe_xS + (2x+3)O_2 \rightarrow xFe_3O_4 + 3SO_2$	F1, P1	Fig. 7
8	$Fe + \frac{1}{2}O_2 \rightarrow FeO$	F1, P1	-
9	$3FeO + \frac{1}{2}O_2 \rightarrow Fe_3O_4$	F0.7, P2	Fig. 6
10	$2Fe_3O_4 + 0.5O_2 \rightarrow 3Fe_2O_3$	F1, P1	Fig. 8
11	$FeCO_3 \rightarrow FeO + CO_2$	An, P1	Fig. 4
12	$CaSO_4(H_2O)_2 \rightarrow CaSO_4 + 2H_2O$	An, P1	Fig. 2
13	$CaSO_4 \rightarrow CaO + SO_2 + 0.5O_2$	F1, P1	Fig. 3
14	$Al_4((OH)_8Si_4O_{10}) \rightarrow 2(Al_2O_3 \cdot 2SiO_2) + 4H_2O$	-	-
15	$3(Al_2O_3 \cdot 2SiO_2) \rightarrow 3Al_2O_3 \cdot 2SiO_2 + 4SiO_2$	-	-
16	all possible phase transformations	EQ	-
17	all possible structural transformations	EQ	-

Under pulverized coal combustion conditions in the radiative section the gas temperature reaches values of 1700 °C, whereas burning char particles are 100 – 300 °C hotter than the surrounding flue gas. Typical residence times and heating rates of 1-3 s, respectively 10^4-10^6 °C/s are reported (Gallagher, 1992), (Neuroth, 2007). The reaction rates vary widely: fast and slow reactions take less than 1 s, respectively several hours to complete. Given the short residence time in combustion chambers the slow reactions are believed to occur in the ash deposits.

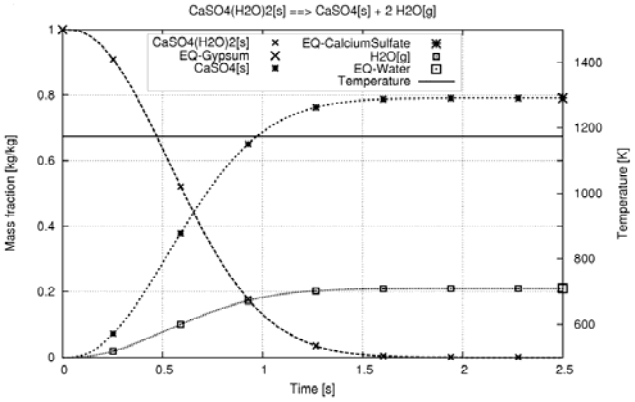

Fig. 2 Gypsum dehydration

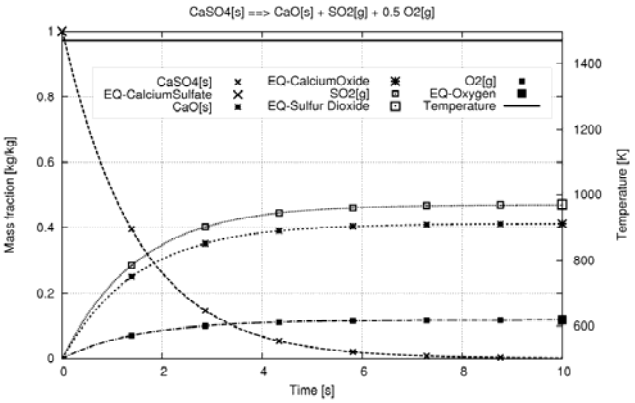

Fig. 3 Anhydrite decomposition

Gypsum ($CaSO_4(H_2O)_2$). Gypsum dehydrates during rapid heating to form anhydrite ($CaSO_4$) and water vapor (Fig. 2).

At high temperatures anhydrite decomposes (Fig. 3) to release SO_2 which further reacts to form very fine particles (Li et al., 2002).

Pure gypsum and anhydrite do not normally form sticky particles inside the combustion chamber. Their presence in deposits is explained by inertial deposition or impaction on sticky surfaces. Calcium and sulfur compounds are reported to form strong bonds on the deposited ash (Fernandez-Turiel et al., 2002).

Siderite ($FeCO_3$). Siderite decomposition is relatively fast (Fig. 4). Its decarbonation starts at temperatures as low as 500 °C (Mukherjee and Srivastava, 2006).

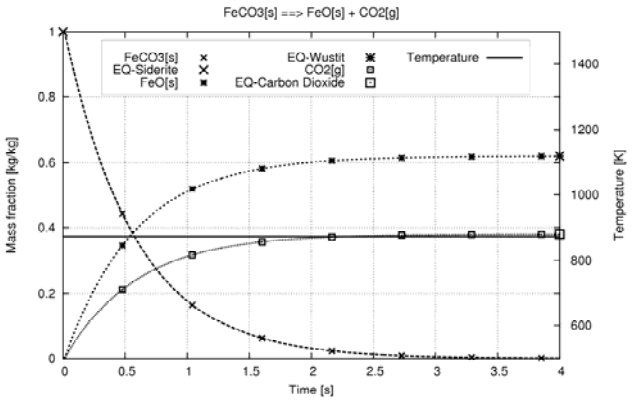

Fig. 4 Siderite decarbonation

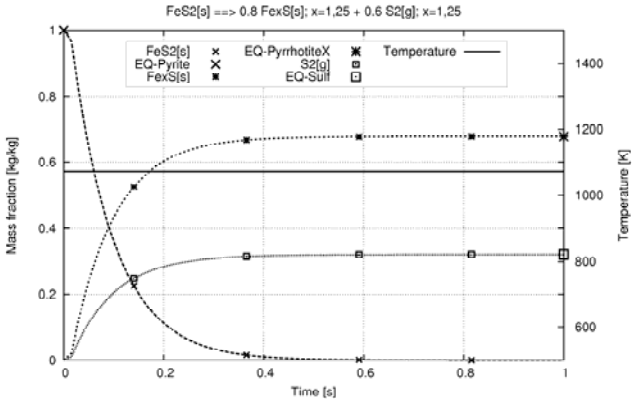

Fig. 5 Pyrite decomposition

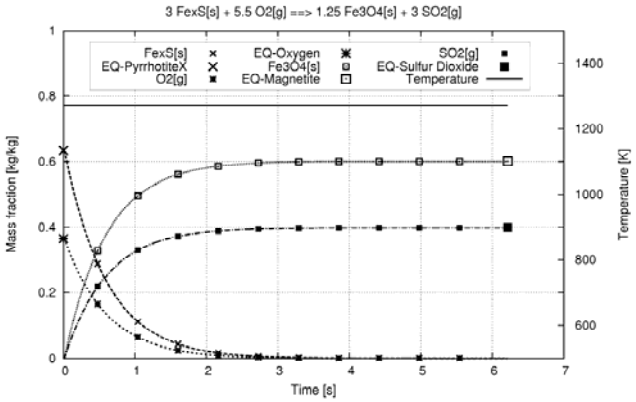

Fig. 6 Pyrrhotite oxidation to magnetite

Pyrite (FeS_2). In an oxidizing environment pyrite undergoes the following transformations:

$$FeS_2 \rightarrow Fe_xS \rightarrow Fe-S-O \rightarrow Fe_3O_4 \rightarrow Fe_2O_3 \quad (26)$$

As shown in Fig. 5, pyrite decomposition to pyrrhotite (Fe_xS) is a fast reaction. Temperatures above 1083 °C cause the porous pyrrhotite particle to melt (Mayoral et al., 2002).

Under reduction conditions pyrrhotite releases sulfur. However, the reaction is slow in comparison to typical particle flight time in combustion chambers (Tomeczek et al., 2004).

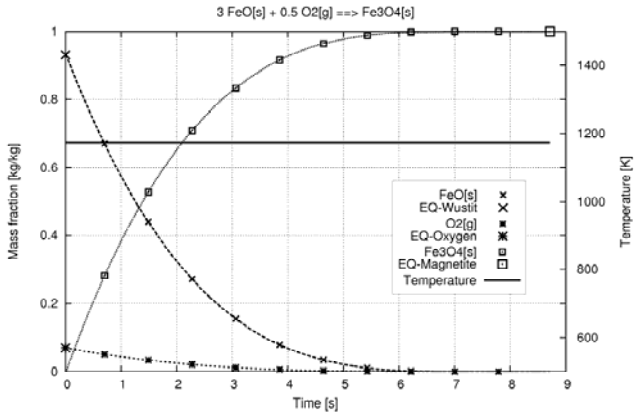

Fig. 7 Magnetite formation

If oxygen diffuses into the pyrrhotite particle than wustite (FeO) and magnetite (Fe_3O_4) (Fig. 6) are formed. Wustite oxidation to magnetite is shown in Fig. 7.

The very low reaction rate of hematite (Fe_2O_3) formation suggests that hematite found in deposits (Neuroth, 2007) is probably the result of iron minerals oxidation after deposition (Fig. 8).

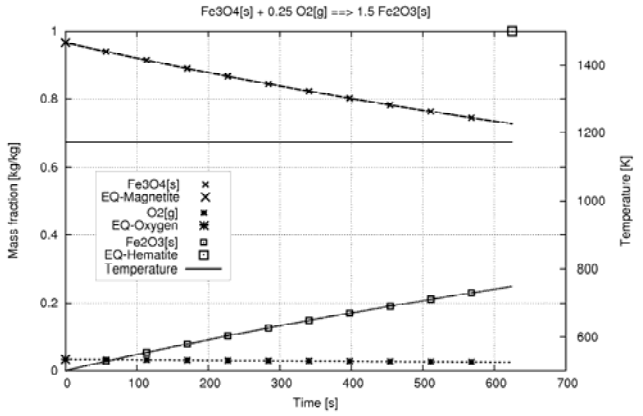

Fig. 8 Magnetite oxidation to hematite

3.3 CFD simulation results and discussion

The combustion chamber and the first section of the flue gas system of the experimental facility were discretized with a 150x120x120 rectangular mesh. The inlet and the walls have a fine cell distribution, while the vertical flue-gas pathway has a coarse one. The chemical analyses of the Hambach coal and operational conditions of the test facility were used as initial and boundary conditions.

Fig. 9 shows the mass flow rate of ash and coal particles deposited on the bottom wall. Since only minor deposits form on the other walls, they are not shown here. As in the experiments, the CFD modeling predicts higher deposition rates in the section A and B of the bottom wall. Therefore, the physical appearance of the CFD calculated deposits is in qualitatively agreement with the experiments. A deposition rate of 690.3 g/h was computed, while a rate of 723 g/h was determined experimentally.

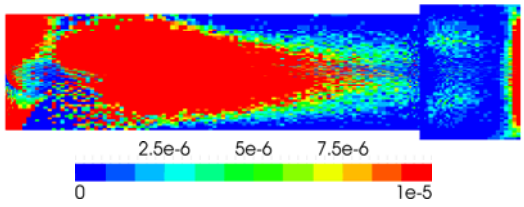

Fig. 9 Mass flow rate of particles (kg/(m^2s)) deposited on the bottom wall

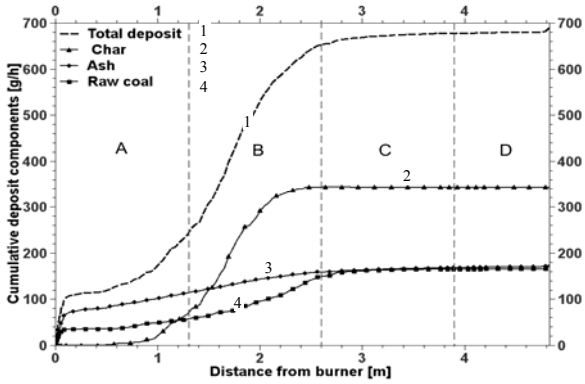

Fig. 10 Mass flow rate of particles deposited to the walls (summed in x direction)

The CFD calculation predicts that the deposit consists of raw coal, unburned char and ash (Fig. 10). The deposit in section A is mainly formed of ash and raw coal particles and accounts for about 34 mass-% of the total deposit.

In section B, with increased particle residence time, as raw coal undergoes pyrolysis, the char becomes the main constituent in particles and deposit.

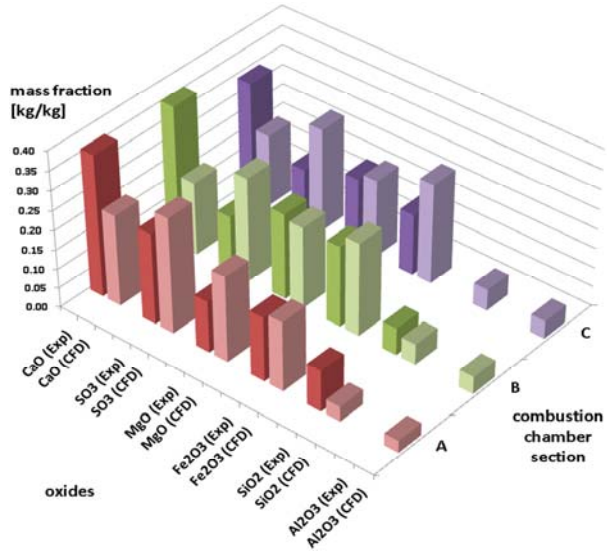

Fig. 11 Chemical analyses of oxides in deposits

Only about 5.5 mass-% of the total amount of deposit accumulates in sections C and D. This is believed to occur due to the intensive particle mass loss (because of pyrolysis, char combustion and MM decomposition). Therefore, the particles are carried by the flue gas to the exit.

Because the modeling does not consider secondary chemical reactions of the MM in the deposit, the composition of the modeled deposit can be compared with the experiments only on basis of the chemical analyses of oxides (Fig. 11). Experimental ash probes were collected only form sections A-C.

The average composition of the deposit changes slightly with increase in distance from the burner (section A-C). The dominant components are CaO, SO_3, MgO, Fe_2O_3, SiO_2 and Al_2O_3. With increased distance from burner, as gypsum and anhydrite particles loose weight due to dehydroxylation, respectively sulfur release (i.e., more particles exit the chamber) the mass fraction of CaO in deposit decreases. The same tendency is observed for SO_3 due to sulfur release form pyrite and anhydrite decomposition.

MgO, SiO_2 and Fe_2O_3 experimental and computational values are in very good agreement. MgO and SiO_2 behave as inert due to the low temperatures in the combustion chamber. The refinement of the iron reactions model which encompasses 11 reactions is thought to be responsible for the very good Fe_2O_3 prediction.

Al_2O_3 was not quantified in the experiments.

4 CONCLUSIONS

The developed CFD model is able to reproduce the observations in a pulverized coal fired test facility. This proves that coal MM transformation can be modeled as a mixture of individual minerals. To improve the accuracy of the model further work is needed, particularly on the refinement of the chemical reaction models.

ACKNOWLEDGEMENT

This work is funded under the Cooretec project by BMWi, EnBW, E.ON, RWE, Vattenfall, Evonik Steag, Alstom Power, Hitachi-Power, AZT Risk & Technology, Salzgitter Mannesmann, Sandvik, ThyssenKrupp VDM, V&M under grant number 0327744A. The project partners: IEK-2 - Forschungszentrum Jülich, IFK/MPA – Uni Stuttgart, EST - TU Darmstadt are gratefully acknowledged for helpful discussions and suggestions.

NOMENCLATURE

Latin letters

A	surface, m^2
A_{pcs}	projected cross sectional area, m²
a_P	specific surface, m²/kg
C	gas concentration, kg/m³
C_D	drag coefficient, dimensionless
Cn	polynomial coefficients, n=1,2, …
c_p	specific heat capacity, kJ/(kg K)
D	diffusion coefficient, m^2/s
E_A,E_{char}	activation energy, kJ/kmol
EQ	equilibrium
F	force, N
f	reaction model, kg/kg
f_m	factor
f(X)	model function
$\bar{g}$	gravitational acceleration, m/s^2 (vector)
H	enthalpy, kJ/kg
K	reaction constant, 1/s
k_{char}	reaction constant, kg/(m²sPa$^{0.5}$)
k_0	frequency factor, 1/s
m	mass, kg
n	order of reaction
Nu	Nusselt number, dimensionless
p	pressure, N/m^2
P_R	product
Pn	polynomial coefficents
Q	heat, kJ
$\dot{Q}$	rate of heat flow, kW
R_C	reactant
R	gas constant, kJ/(kmolK)
Re	Reynolds number, dimensionless
r	radius, m
r_{H2O}	heat of vaporization, kJ/kg
S	entropy, kJ/K
T	temperature, K
$\bar{u}$	velocity, m/s (vector)
V	volume, m^3
x	pathway, m
X_i	volume fraction of species i, m^3/m^3
Y_i	mass fraction of species i, kg/kg
Z	volume change, m^3/m^3

Greek symbols

β	heating rate, K/s
Δ	difference
μ	dynamic viscosity, kg/(ms)
ν	stoichiometric coefficient, dimensionless
ρ	density, kg/m^3
τ	time, s
τ_D	particle relaxation time, s

Subscript

c	core	mi	mineral
chem	chemical	p	particle
comb	combusted	por	porosity
cond	conduction	pyr	pyrolysis
conv	convection	R	reactant
d	diameter	vol	volatiles
daf	dry and ash free	rad	radiation
eff	effective	0	reference
g	gas	x,y	stoichiometric coefficients
melt	melting		

REFERENCES

Bailey, C. W., Bryant, G. W., Matthews, E. M., and Wall, T. F., 1998 Investigation of the high-temperature behavior of excluded siderite grains during pulverized fuel combustion. Energy & Fuels, Vol. 12, pp. 464–469.

Bonn, B., 2010, Charakterisierung von Kohlenaschen hinsichtlich ihrer Verschlackung in Dampferzeugern. *VGB PowerTech*, Vol. 8, pp. 58–65.

Bozic, O. Leithner, R., Müller, H., 2000, Calculation of the Mineral Matter Transformations in Coal Fired Furnaces to Simulate Slagging Potential, *Proc. 12th International Conference on Coal Research*, Sandton, South Africa.

Bozic, O., 2003, Numerische Simulation der Mineralumwandlung in Kohlenstaubfeuerungen, PhD Thesis, *TU Braunschweig.*

Bailey, C. W., Bryant, G. W., Matthews, E. M., and Wall, T. F., 1998, Investigation of the high-temperature behavior of excluded siderite grains during pulverized fuel combustion, *Energy & Fuels*, Vol. 12, pp. 464–469.

Epple, B., Leithner, R., Linzer, W. and Walter, H., 2009, Simulation von Kraftwerken und wärmetechnischen Anlagen*, Springer,* ISBN: 978-3-211-29695-0.

Erickson, T., Allan, S., McCollor, D., Hurley, J., Srinivasachar, S., Kang, S., Baker, J., Morgan, M., Johnson, S. and Borio, R., 1995, Modelling of fouling and slagging in coal-fired utility boilers. *Fuel Processing Technology*, Vol. 44, pp. 155–171.

Fernandez-Turiel, J. L., Georgakopoulos, A., Gimeno, D., Papastergios, G. and Kolovos, N., 2002, Ash Deposition in a Pulverized Coal-Fired Power Plant after High-Calcium Lignite Combustion. *Energy Sources*, Vol. 24, pp. 561-573.

Field, M. A. et al., 1967, Combustion of pulverised coal, *BcURA*, Leatherhead, England.

Fischer, K. C., 1998, Dreidimensionale Simulation der Gas-Fest-Stoffströmung in kohlegefeuerten Dampferzeugern, PhD Thesis, *TU Braunschweig*.

Gallagher, N. B., 1992, Alkali metal partitioning in a pulverized coal combustion environment, PhD Thesis, *University of Arizona*.

Hecken, M., Reichelt, L. and Renz, U., 2001, Numerical Simulation of Slagging Films in the Aachen Pressurized Coal Combustion Facility. *Developments in Chemical Engineering and Mineral Processing*, Vol. 9, pp. 239-251.

Kingery, W. D., Bowen, H. K. and Uhlmann, D. R., 1976, Introduction to Ceramics; *Wiley*, New York.

Lee, F. and Lockwood, F., 1998, Modelling ash deposition in pulverized coal-fired applications. *Progress in Energy and Combustion Science*, Vol. 25, pp. 117–132.

Leithner, R., Müller, H., 2003a, CFD studies for boilers, *Second M.I.T. Conference on Computational Fluid and Solid Mechanics,* Cambridge, USA.

Leithner, R., Neuroth, M., Bozic, O., Hoppe, A., 2003b, Einfluß von Verschlackung und Verschmutzung auf Kohleauswahl, Dampferzeugerauslegung und -betrieb - Erfahrungen und Simulation, *21. Deutscher Flammentag: VDI-Bericht 1750*, Cottbus.

Li, Y., Loh, B. C., Matsushima, N., Nishioka, M. and Sadakata, M., 2002, Chain reaction mechanism by NO_x in SO_2 removal process. *Energy and Fuels*, Vol. 16, pp. 155–160.

Lockwood, F. C. Costen, P. G., Siddiqi, M. M., Harrison, P. J., Mineral Ash Transformation. *The Imperial college of Science, Technology and Medicine,* Report JOF3-CT95-0024.

Magda, A., Magda, S., Strelow, M., and Leithner, R., 2009, Mineral Matter Issues in Coal-Fired Power Plants. *Joint Meeting of the Scandinavian-Nordic and French Sections of the Combustion Institute*, Copenhagen, Denmark.

Mayoral, M. C., Izquierdo, M. T., Andrés, J. M. and Rubio, B., 2002, Mechanism of interaction of pyrite with hematite as simulation of slagging and fireside tube wastage in coal combustion. *Thermochimica Acta*, Vol. 390, pp. 103–111.

McBride, B., Gordon, S., and Reno, M., 1993, Coefficients for calculating thermodynamic and transport properties of individual species, *NASA*, Report 4513.

McIntosh, M. J., 1976, Mathematical model of drying in a brown coal mill system. 1. Formulation of model. *Fuel*, Vol. 55, pp. 47–52.

Mukherjee, S. and Srivastava, S. K., 2006, Minerals transformations in northeastern region coals of India on heat treatment. *Energy and Fuels*, Vol. 20, pp 1089-1096.

Müller, H., 1992, Numerische Berechnung dreidimensionaler turbulenter Strömungen in Dampferzeugern mit Wärmeübergang und chemischen Reaktionen am Beispiel des SNCR-Verfahrens und der Kohleverbrennung, *VDI-Fortschrittsberichte Reihe 6: Energieerzeugung,* Nr. 268.

Neuroth, M., 2007, Thermochemische Simulation und experimentelle Untersuchungen zur Ansatzbildung in Kohledampferzeugern am Beispiel rheinischer Braunkohle, *RWE Power AG,* Report.

Richards, G., Slater, P. and Harb, J., 1993, Simulation of ash deposit growth in a pulverized coal-fired pilot scale reactor, *Energy & Fuels*, Vol. 7, pp. 774–781.

Schiller, L. and Nauman, A., 1935, A drag coefficient correlation. *V.D.I. Zeitung*, Vol. 77, pp. 318–320.

Schubert, H., 1977, Mechanische Verfahrenstechnik, *Deutscher Verlag für Grundstoffindustrie*, VEB, Leipzig.

Tanaka, H., 1995, Thermal analysis and kinetics of solid state reactions, *Thermochimica Acta*, Vol. 267, pp. 29–44.

Tomeczek, J., Palugniok, H. and Ochman, J., Modelling of deposits formation on heating tubes in pulverized coal boilers, *Fuel*, Vol. 83, pp. 213–221.

Vyazovkin, S. and Wight, C. A., 1997, Kinetics in Solids. *Annual Reviews in Physical Chemistry*, Vol. 48, pp. 125–149.

Wag, K., Reis, V., Frederick, W. and Grace, T., 1997, Mathematical model for the release of inorganic emissions during black liquor char combustion. *Tappi Journal*, Vol. 80, pp. 135–145.

Wei, X. and Lopez, C. and von Puttkamer, T. and Schnell, U. and Unterberger, S. and Hein, K.R.G., 2002, Assessment of chlorine-alkali-mineral interactions during co-combustion of coal and straw, *Energy & fuels,* Vol. 16, pp. 1095-1108

Wilemski, G. and Srinivasachar, S., 1993, Prediction of ash formation in pulverized coal combustion with mineral distribution and char fragmentation models. The Impact of Ash Deposition on Coal Fired Plants, *Taylor & Francis*, pp. 151–164.

Wörner, M., 2003, A compact introduction to the numerical modeling of multiphase flows, *Wissenschaftliche Berichte FZKA*, Report 6932.

Yan, L., Gupta, R. and Wall, T., 2002, A mathematical model of ash formation during pulverized coal combustion, *Fuel*, Vol. 81, pp. 337–344.

Zevenhoven, M. and Backman, R., 1998, The Chemistry of Biomass Ashes in Pressurised Gasification. Part II, *Abo Akademi University*, Report 98-2.